Downloaded from rsta.royalsocietypublishing.org

PHILOSOPHICAL TRANSACTIONS OF THE ROYAL SOCIETY A MATHEMATICAL, PHYSICAL & ENGINEERING SCIENCES

Grain boundary evolution and continuous recrystallization of a superplastic Al––Cu––Zr alloy

Terry R. McNelley, Michael E. McMahon and M. Teresa Pérez Prado

Phil. Trans. R. Soc. Lond. A 1999 **357**, 1683-1705
doi: 10.1098/rsta.1999.0396

Email alerting service

Receive free email alerts when new articles cite this article - sign up in the box at the top right-hand corner of the article or click **here**

To subscribe to *Phil. Trans. R. Soc. Lond. A* go to: **http://rsta.royalsocietypublishing.org/subscriptions**

This journal is © 1999 The Royal Society

Downloaded from rsta.royalsocietypublishing.org

THE ROYAL SOCIETY

Grain boundary evolution and continuous recrystallization of a superplastic Al–Cu–Zr alloy

By Terry R. McNelley[1]†, Michael E. McMahon[1]† and M. Teresa Pérez-Prado[2]

[1]*Department of Mechanical Engineering, Naval Postgraduate School, 700 Dyer Road, Monterey, CA 93943-5146, USA*
[2]*Departamento de Metalurgia Fisica, Centro Nacional de Investigaciones Metalúrgicas (CENIM), Avda. Gregorio del Amo, 8-28040 Madrid, Spain*

Two distinct microstructural transformation processes have been observed to enable superplastic response in aluminium alloys, depending upon the composition and thermomechanical history. Continuous recrystallization has been used to describe the transformation leading to a superplastically enabled state in alloys that respond to processing, as does the commercial alloy Supral 2004. Such a transformation is characterized by significant retention of the deformation microstructure and texture. Microtexture analysis methods have been employed to examine the grain-boundary misorientation distribution in as-processed Supral 2004, and its evolution during annealing of this alloy. A bimodal boundary misorientation distribution is observed in as-processed material and is seen to persist through subsequent annealing. Comparison of correlated (nearest neighbour) with uncorrelated (predicted by the texture) grain-boundary misorientation data reveals that the populations of boundaries in the misorientation ranges of 0–15° and 55–62.8° exceed those predicted. A model is presented describing high-angle boundaries as interfaces between symmetric variants of the deformation texture components. The misorientation distribution of lower-angle boundaries can be fitted by a probability density function. It is concluded that grain subdivision into deformation bands during severe straining leads to the formation of high-angle grain boundaries as interfaces between symmetric variants of deformation texture components, while lower-angle boundaries develop by dislocation reaction within these variants, leading to observed bimodal grain-boundary misorientation distributions. During post-processing static annealing, stable coarsening of deformation-induced features occurs gradually and homogeneously throughout the microstructure without recrystallization involving the formation of new grains by the migration of high-angle grain boundaries. The ability to quantify and model the reactions that occur during thermomechanical processing, and that lead to the microstructures present in Supral 2004, will facilitate processing for similar reactions in a wider family of aluminium alloys for enhanced formability.

Keywords: deformation processing; superplasticity; Supral; grain boundaries; boundary misorientation; continuous polycrystallization

† US Government work not protected by US copyright.

© 1999 The Royal Society
TEX Paper

PHILOSOPHICAL TRANSACTIONS OF THE ROYAL SOCIETY A MATHEMATICAL, PHYSICAL & ENGINEERING SCIENCES
PHILOSOPHICAL TRANSACTIONS OF THE ROYAL SOCIETY A MATHEMATICAL, PHYSICAL & ENGINEERING SCIENCES

Downloaded from rsta.royalsocietypublishing.org

1. Introduction

The present understanding of microstructural control in engineering alloys during industrial processing by deformation and recrystallization is largely empirical in nature. The ability to predict and then produce required microstructures for specific applications, such as superplastic forming, is limited, and this is reflected in the limited range of superplastic aluminium alloys available for engineering applications. Currently, two alternative processing procedures have been established to generate superplastic microstructures in wrought aluminium alloys.

The procedure of interest here was initially developed for Zr-containing materials such as Supral 2004 (nominally 6.0 wt% Cu–0.5 wt% Zr), and involves deformation processing of as-cast material by only warm (*ca.* 300 °C) and cold rolling in order to retain a very fine dispersion of Al_3Zr (Grimes 1988; Watts *et al.* 1976). Upon heating to the forming temperature, the presence of fine Al_3Zr particles apparently retards the formation and migration of high-angle boundaries in the deformation microstructure. Thus, recrystallization (as normally defined) is suppressed, and so recovery processes predominate in the evolution of a refined superplastically enabled microstructure. These processes are believed to involve subgrain-boundary formation uniformly throughout the microstructure, with the build-up of boundary misorientation by incorporation of dislocations as well as by boundary coalescence. The strain-rate sensitivity of the flow stress increases during initial stages of straining at superplastic forming temperatures and strain rates (typically 450 °C and 10^{-2} s^{-1}), and this transition to a superplastic state has been attributed to dynamic continuous recrystallization. Such a reaction is thought to involve a further strain-induced progressive increase in the misorientation of subgrain boundaries that initially developed by recovery during prior annealing (Grimes 1988; Watts *et al.* 1976; Bricknell & Edington 1979; Edington 1982).

X-ray texture analysis and TEM methods have not provided conclusive evidence for such processes. Instead, discrete measurement of grain orientation using electron backscatter diffraction (EBSD) techniques suggests that boundary misorientations become established in the cellular deformation-induced structures in as-processed material (McNelley & McMahon 1997). Then, continuous recrystallization processes during annealing result in the retention of cellular dislocation structures developed during thermotechnical processing (TMP), accompanied by sharpening of the cell boundaries. During superplastic straining, evidence of the onset of grain-boundary sliding is the randomization of grain orientation and a reduction in texture (McNelley & McMahon 1997; Pérez-Prado *et al.* 1998). Further data are needed on the development and evolution of grain boundaries during processing, annealing and straining. Newly developed computer-aided EBSD methods (see, for example, Randle 1992) have been employed in this laboratory to investigate the effects of deformation processing, annealing and elevated-temperature deformation on the microstructures and grain-boundary characteristics of several superplastic Al-based alloys (McNelley & McMahon 1996*a*, *b*, 1997; Pérez-Prado *et al.* 1998; McMahon 1996; McNelley *et al.* 1997).

The format of this paper is as follows. First, we review the current understanding of grain refinement and deformation processing for superplasticity in aluminium. An interactive EBSD method (McNelley & McMahon 1996*a*, *b*; McMahon 1996) of investigation will then be briefly reviewed, followed, finally, by consideration of micro-

Downloaded from rsta.royalsocietypublishing.org

texture in as-processed Supral 2004, and its evolution during subsequent annealing. The goal is to provide better insight into development of grain boundaries during processing and the relationship between deformation processing, texture and grain boundaries for this superplastic aluminium alloy.

2. Grain refinement and deformation processing for superplasticity: a review

The recognized requirements for fine-grain superplasticity in aluminium alloys include a high value of m, the strain-rate sensitivity coefficient of the flow stress, due to deformation at temperatures and strain rates where grain-boundary sliding is dominant during deformation. Grain-boundary sliding must be accommodated by either slip- or stress-directed diffusion, and together these processes constitute the mechanism of superplasticity. For this, grains must be equiaxed and highly refined, with mobile grain boundaries that can slide while resisting tensile separation (Grimes 1988; Sherby & Wadsworth 1982; Nieh *et al*. 1997).

The mechanical behaviour of fine-grained superplastic materials may be described by a constitutive law involving additive contributions of independent superplastic and dislocation creep mechanisms (Sherby & Wadsworth 1982; Nieh *et al*. 1997; Sherby & Burke 1968). Thus,

$$\dot{\varepsilon}_{\text{total}} = \dot{\varepsilon}_{\text{sp}} + \dot{\varepsilon}_{\perp}, \tag{2.1}$$

where $\dot{\varepsilon}_{\text{total}}$ is the observed total strain rate, and $\dot{\varepsilon}_{\text{sp}}$ and $\dot{\varepsilon}_{\perp}$ are the contributions of the superplastic and the dislocation creep mechanisms, respectively, to the total strain rate. Grain-boundary sliding and its accommodation mechanisms are envisioned to occur within the grain boundaries and in adjacent, mantle-like regions of the grains; accordingly, $\dot{\varepsilon}_{\text{sp}}$ is strongly grain-size dependent. The dislocation creep process is usually presumed to occur independently in the core regions of the grains and so $\dot{\varepsilon}_{\perp}$ is unaffected by changes in grain size. Studies of the effects of strain rate, temperature, alloy constitution and microstructure on elevated temperature deformation behaviour of metallic materials have resulted in various phenomenological constitutive equations for these mechanisms (see, for example, Sherby & Wadsworth 1982; Nieh *et al*. 1997; Sherby & Burke 1968). Here, two of these relationships may be combined (Nieh *et al*. 1997) to give

$$\dot{\varepsilon}_{\text{total}} = AD^{*}_{\text{eff}}\left(\frac{1}{d}\right)^{2}\left(\frac{\sigma}{E}\right)^{2} + KD\left(\frac{\sigma}{E}\right)^{n}, \tag{2.2}$$

where A is a material constant for the superplastic mechanism, D^{*}_{eff} is a modified effective diffusion coefficient, d is the grain size, σ is the applied stress and E is Young's modulus; K is a material constant for the dislocation creep mechanism, and D and n are the appropriate diffusion coefficient and n stress exponent for the dislocation creep mechanism. Depending on the specific dislocation mechanism, the stress exponent, n, may have values ranging from 3 to 5.

Equation (2.2) predicts a grain-size-dependent transition in dominant mechanism, from dislocation creep for high values of the stress and strain rate to slip- or diffusion-accommodated grain-boundary sliding at lower values of the stress and strain rate. This can be readily seen for a hypothetical case where $D^{*}_{\text{eff}} = D$ (the lattice diffusivity) and $n = 5$ (i.e. dislocation climb-controlled creep); then, equation (2.2) can

Downloaded from rsta.royalsocietypublishing.org

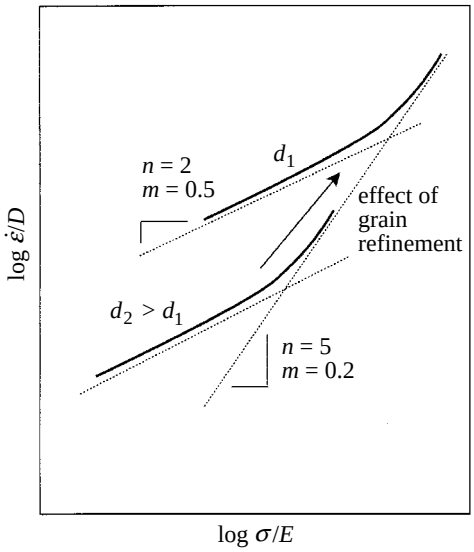

Figure 1. A schematic representation of the effect of grain size refinement on the transition from dislocation creep control to slip- or diffusion-accommodated grain-boundary sliding control of deformation. The latter mechanisms are responsible for superplastic behaviour. Grain refinement increases the strain-rate range for superplastic behaviour and improves the superplastic response.

be plotted as diffusion-compensated strain rate, $\dot{\varepsilon}/D$, versus modulus-compensated stress, σ/E. For independent deformation mechanisms, the fastest will be rate controlling; this is shown by the solid lines in the representation of figure 1. The transition to superplastic behaviour occurs as the apparent stress exponent decreases, from $n \approx 5$ to $n \approx 2$. Since $m = 1/n$, the strain-rate sensitivity coefficient increases from $m \approx 0.2$ to $m \approx 0.5$. This latter value is usually regarded as sufficient to support extensive superplastic response (Sherby & Wadsworth 1982; Nieh *et al*. 1997). Clearly, a finer grain size increases the strain rate at which this transition is expected to occur. Indeed, this is the basis for the requirement that the grain size, d, must be less than 10 μm for useful superplastic response in metallic materials. Superplasticity also requires that the deformation temperature must exceed $0.5T_{\mathrm{M}}$, where T_{M} is the melting temperature, because of the role of diffusion. At such temperatures, concurrent grain growth during superplastic straining will tend to suppress superplastic response. Thus, provision for stabilization of grain size is also necessary in the design of alloys and processes for superplasticity.

The assertion is often made (see, for example, Sherby & Wadsworth 1982; Nieh *et al*. 1997) that high-angle grain boundaries are also necessary for superplasticity. However, little work has been reported on the relationship between grain-boundary characteristics such as the misorientation distribution and grain-boundary sliding in polycrystalline materials. In an Al–Mg–Zr alloy, the peak superplastic ductility was shown to have improved dramatically as processing parameters were adjusted to increase the population of 5–15° boundaries in the misorientation distribution (McNelley & McMahon 1996*b*). Such distributions can now be readily evaluated in superplastic aluminium alloys (e.g. Randle 1992; McMahon 1996; McNelley & McMahon 1996*a*, *b*; McNelley & McMahon 1997; McNelley *et al*. 1997; Pérez-Prado

Downloaded from rsta.royalsocietypublishing.org

et al. 1998) and so the interactions among thermomechanical processing parameters, grain-boundary characteristics and superplasticity may now be quantified.

In alloys of iron or titanium, achieving the necessary grain refinement is greatly facilitated by the phase transformations that occur during cooling of these metals. For all other metallic alloys, including those based on copper and nickel as well as aluminium, the required grain refinement may be achieved only by recrystallization after plastic deformation. During deformation processing, strain energy is stored in a deformation-induced structure consisting mainly of dislocations; this stored energy may be released by the processes of recovery, recrystallization, and grain growth. Recovery is generally considered to involve dislocation rearrangement in the absence of high-angle boundary migration while recrystallization is usually defined as the formation and subsequent migration of high-angle boundaries that separate old, deformed material from new, strain-free material (Doherty *et al*. 1988). The kinetic theory of nucleation during phase transformations as it applies to recrystallization has recently been reviewed (Doherty *et al*. 1997). The standard model of nucleation by thermal fluctuation considers that the energy barrier, ΔG^*, between the old and new structures is related to the volume free-energy difference, ΔG_v, the interfacial energy, γ, and the contact angle, λ (for nucleation on a pre-existing defect interface) by

$$\Delta G^* = \frac{\kappa\gamma^3}{\Delta G_\mathrm{v}^2} f(\cos\lambda), \tag{2.3}$$

where κ is a nucleus shape factor equal to $16\pi/3$ for an isolated sphere. This model agrees well with experimental behaviour for a wide range of phenomena including several types of solid-state reactions, but it is inadequate for the case of recrystallization. The relatively low values of stored strain energy due to deformation result in $\Delta G_\mathrm{v} \approx 0.5$–$5.0$ MPa. For a high-angle boundary, the interfacial energy $\gamma \approx 0.5$ J m^{-2} and hence ΔG^* is so large, of the order of $10^5 kT$, that the nucleation rate of new grains would be zero at any temperature up to the melting point of the material. An alternative view is that the observed rates of formation of new grains are many orders of magnitude larger than predicted by the thermal fluctuation model.

Because of this it is now recognized that new grain nuclei do not form by the coalescence of individual atoms as envisioned in the standard model. Instead, new grains may grow from small cells or subgrains that constitute embryos already present in the deformation microstructure. This may account for the observation that the orientations of new, recrystallized grains evolve from the orientations of the embryos present in the deformed state. Recently, the stability during annealing of such fine, cellular structures as are produced during deformation processing of metals has been investigated and it has been shown that they may transform in either of two ways (Humphreys 1997). One involves an apparently unstable growth of isolated cells heterogeneously within the deformation microstructure. Such unstable growth may result if isolated cells are highly misoriented (and therefore have high interfacial energy) with their nearest-neighbour cells. This would appear as a nucleation and growth process in that it involves seemingly extensive structural changes that are spatially localized initially and also have distinct interfaces between old and new structures. Recrystallization via particle-stimulated nucleation (PSN) in Al–Zn–Mg–Cu alloys (Humphreys 1977; Paton & Hamilton 1978; Wert *et al*. 1981) and abnormal grain growth are reactions of this type because there appear to be distinct formation and growth processes, although it is now understood that the recrystallization

Downloaded from rsta.royalsocietypublishing.org

Table 1. *Alloy composition (wt%) for the as-received SUPRAL 2004*

	Cu	Zr	Fe	Si	Zn	Mn	Mg	Ti	Li	Al
cast no. 2004F013	5.66	0.37	0.14	0.06	0.029	0.013	0.003	0.005	0.0001	bal

embryos were developed during prior plastic deformation and not by thermal fluctuation.

Microstructures developed from such discontinuous recrystallization reactions have essentially strain-free grains with predominantly disordered, high-angle grain boundaries having high interfacial energy. These boundaries tend to be highly mobile and, as a result, grain growth occurs readily at elevated superplastic forming temperatures, suppressing the superplastic response and formability.

The other way of transformation consists of stable, homogeneous coarsening of the cellular deformation microstructure. Stable coarsening is favoured if, on average, the cellular structures are relatively highly misoriented and characterized by a narrow range of grain misorientation (Humphreys 1997). This would be consistent with continuous recrystallization reactions, which involve changes that are initially small in magnitude but that occur in a homogeneous manner throughout the microstructure. Transformations involving primarily recovery and recovery-dominated processes such as those occurring in Supral apparently occur in this fashion. It is noted that, other than in non-engineering eutectic alloys studied in early research, aluminium alloys which transform by homogeneous reactions generally have exhibited better superplastic responses than those which transform by discontinuous reactions. This probably reflects generally finer but more stable grain structures associated with the homogeneous reactions.

In the aforementioned treatment of microstructural instability, boundary energies and mobilities were assumed to be related only to the local misorientations of the cell boundaries. Although many other factors also contribute to the onset of recrystallization (Doherty *et al*. 1997) the foregoing provides a framework for analysis of grain-boundary character and its evolution during annealing in this Al–Cu–Zr alloy leading to the ability to support superplastic flow. A model which describes the formation of refined dislocation structures during severe deformation of metals and alloys has yet to emerge and so a complete description of the grain-boundary characteristics and transformation behaviour in such a material remains to be developed.

3. Experimental

Supral 2004 material was obtained as 2.0 mm sheet in the as-processed condition from Superform-USA, Inc. Chemical composition data are provided in table 1. Details of processing are proprietary; chill casting is employed to avoid formation of primary Al_3Zr and subsequent homogenization treatments are conducted at lower than normal temperatures to inhibit precipitation of Zr. Deformation processing by hot rolling to a strain of about 2.0 is then followed by cold cross rolling to an additional strain of about 1.0. The as-processed material exhibits a tensile elongation of *ca.* 800% upon heating and straining at 450 °C and strain rates up to $10^{-2}\ s^{-1}$.

Coupons of as-processed material and material given annealing treatments at 450 °C for times varying from 30 min to 12 h were prepared for EBSD examina-

Downloaded from rsta.royalsocietypublishing.org

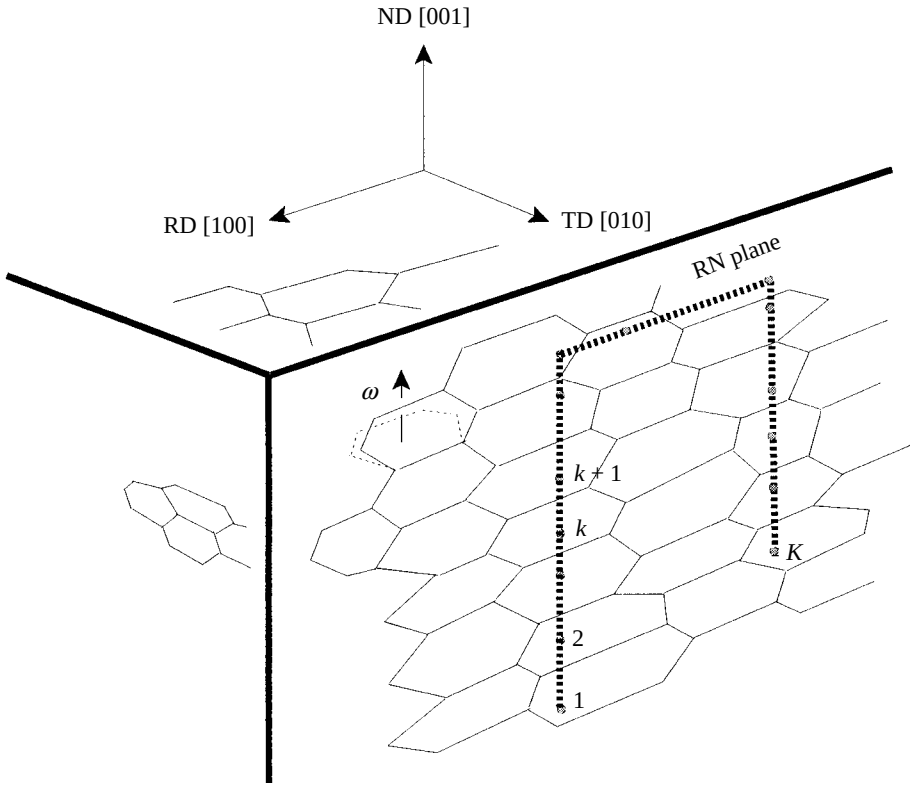

Figure 2. A schematic of the data collection procedure, showing a traverse consisting of linear segments along which orientation measurements are made with each change in the observed diffraction pattern. The correlated misorientation distribution is obtained by evaluating the orientation differences between successive measurements, i.e. k to $k+1$. The uncorrelated misorientation distribution compares any one measured orientation to all others, i.e. k to $1 = 1 \ldots K$, $k \neq 1$.

tion at locations near the midplane of the rolled sheet. A thorough background on EBSD examination is available (Randle 1992). Specific procedures employed here have been described previously (McMahon 1996; McNelley & McMahon 1996*a*, *b*; McNelley & McMahon 1997; McNelley *et al*. 1997; Pérez-Prado *et al*. 1998). Essentially, diffraction patterns are obtained along a linear traverse on a selected plane of examination as illustrated in the schematic of figure 2. The electron beam of the SEM, operating in the spot mode, is initially positioned and a diffraction pattern is captured, automatically indexed and stored by the system software (TexSEM Laboratories, Inc., Provo, UT). The data are in the form of the three Euler angles, ϕ_1^1, Φ^1, and ϕ_2^1, that specify the orientation of crystal 1 relative to axes associated with the final cold rolling stage of the prior TMP. These angles are defined according to Bunge's format (Bunge 1982). The electron beam is then moved, pixel by pixel, until a new diffraction pattern is observed, collected, indexed and the corresponding data also stored; this process is repeated until K (typically 300–500) orientations have been acquired. The distance between successive patterns is also recorded. The

Downloaded from rsta.royalsocietypublishing.org

resulting microtexture data may be displayed in various forms including discrete pole figures or orientation distribution functions.

The successive diffraction patterns correspond to the orientations of *adjacent* grains and so the misorientation of the intervening boundary may be calculated as the minimum rotation angle about an associated axis to bring the neighbouring crystals into coincidence. Complete specification of the boundary would also require the determination of the orientation of the boundary plane (denoted by ω in figure 2) but the additional difficulties in such measurements would severely restrict the quantity of related orientation data. For the kth grain, the matrix

$$A_k = \begin{pmatrix} a_{11}^k & a_{12}^k & a_{13}^k \\ a_{21}^k & a_{22}^k & a_{23}^k \\ a_{31}^k & a_{32}^k & a_{33}^k \end{pmatrix}, \tag{3.1}$$

describes the orientation of the cubic lattice with respect to the reference axes of the processed material. The matrix elements are functions of the Euler angles, ϕ_1^k, Φ^k, and ϕ_2^k, for this grain (Randle 1992).

A similar matrix is obtained in terms of the Euler angles for an *adjacent* grain, i.e. A_{k+1}, in terms of ϕ_1^{k+1}, Φ^{k+1}, and ϕ_2^{k+1}, and the misorientation, or orientation difference between the two grains, may be calculated in terms of the rotation matrix,

$$M_{k,k+1} = A_k^{-1} A_{k+1}, \qquad k = 1 \ldots K-1. \tag{3.2}$$

For K orientation measurements, there will be $K-1$ misorientation matrices; the rotation axes, $R_{k,k+1} = (r_1^{k,k+1}, r_2^{k,k+1}, r_3^{k,k+1})$, and misorientation angles, $\theta_{k,k+1}$, may be obtained (Randle 1992) from the elements of these misorientation matrices as

$$\left.\begin{aligned} r_1^{k,k+1} &= m_{23}^{k,k+1} - m_{32}^{k,k+1}, \\ r_2^{k,k+1} &= m_{31}^{k,k+1} - m_{13}^{k,k+1}, \\ r_3^{k,k+1} &= m_{12}^{k,k+1} - m_{21}^{k,k+1}, \\ \theta_{k,k+1} &= \arccos[\tfrac{1}{2}(m_{11}^{k,k+1} + m_{22}^{k,k+1} + m_{33}^{k,k+1} - 1)]. \end{aligned}\right\} \tag{3.3}$$

It is noted that $\theta_{k,k+1}$ is the minimum when crystal symmetry is taken into account. When defined according to equation (2.3) these are referred to as *correlated* misorientations as the $M_{k,k+1}$ are always the orientation differences between adjacent grains.

Orientation differences between the kth grain and all other grains in the assemblage may be calculated as

$$M_{k,l} = A_k^{-1} A_l, \qquad k,l = 1 \ldots K \quad (k \neq l) \tag{3.4}$$

and the corresponding angles, $\theta_{k,l}$, and axes, $R_{k,l}$, calculated as in equation (3.3). For K individual orientation measurements, this procedure would result in $(K-1)^2$ misorientations although only $(K(K-1))/2$ are distinct. The misorientations calculated according to equation (3.4) are *uncorrelated* misorientations because the grains generally do not share a common boundary. Differences between the distributions of correlated and uncorrelated misorientation measurements may reflect grain-to-grain interactions during deformation and annealing. The distribution of the uncorrelated misorientations, $M_{k,l}$, for K orientation measurements is the discrete analogue to the

Downloaded from rsta.royalsocietypublishing.org

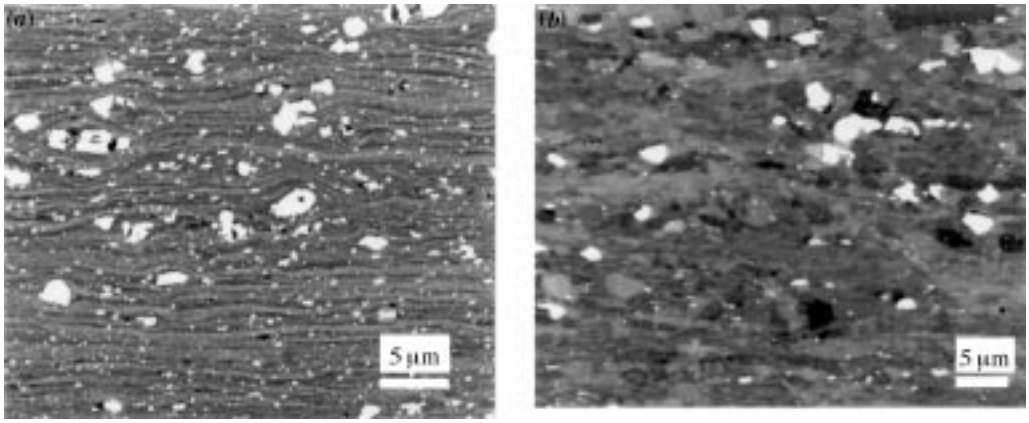

Figure 3. Microstructures of Supral 2004 in (*a*) the as-processed condition and (*b*) following processing and annealing for 30 min at 450 °C. The RN plane of the rolled sheet is shown; the rolling direction is horizontal. BSE images, orientation contrast, no etchant.

continuous misorientation distribution function (MDF), g, which may be calculated from the texture (Adams 1986; Pospiech *et al*. 1986).

The misorientation distributions of the grain boundaries (both correlated and uncorrelated) may then be represented by histograms of relative number versus misorientation angle. The crystal axes of relative rotation for the adjacent lattices were also determined and are displayed within a unit triangle as a grain misorientation texture, or GMT (Randle 1992). Finally, backscattered electron (BSE) micrographs were obtained of the regions examined.

4. Results

Microstructures of as-processed and processed and annealed materials are shown in figure 3. The BSE micrograph of the as-processed material, figure 3*a*, shows a dispersion of coarse Θ (Al_2Cu) particles and a highly directional banded microstructure due to mechanical fibring introduced in the warm and cold rolling processes. The original grains have become flattened to a thickness of *ca.* 3.0 μm in the normal direction, and elongated in the rolling direction; no distinct boundaries are apparent. Following a 30 min anneal at 450 °C, figure 3*b*, a refined substructure 0.5–2.0 μm in size has become apparent between the bands remaining from the as-processed condition. Further annealing resulted only in the development of a uniform, fine substructure, of 2.0–2.1 μm mean linear intercept, and slightly elongated in the rolling direction.

Microtexture data for the as-processed material are shown in the discrete Euler plot of figure 4*a* and comprise a deformation texture. While several components along the β-fibre, including S and $\{123\}\langle 634\rangle$, are present, the brass (Br) component and nearby orientations related to Br by rotations about the sheet normal (i.e. orientations lying along the α-fibre) are most prominent and will be of particular interest here. Grain boundary data for this as-processed condition are presented in figure 4*b* and a bimodal distribution of correlated misorientation angles is apparent in the histogram. Successive orientation measurements were obtained at 0.5 μm spacings, which is less than the reduced thickness of the original grains, and so these data must reflect mainly the distribution of misorientations within a refined, cellu-

Downloaded from rsta.royalsocietypublishing.org

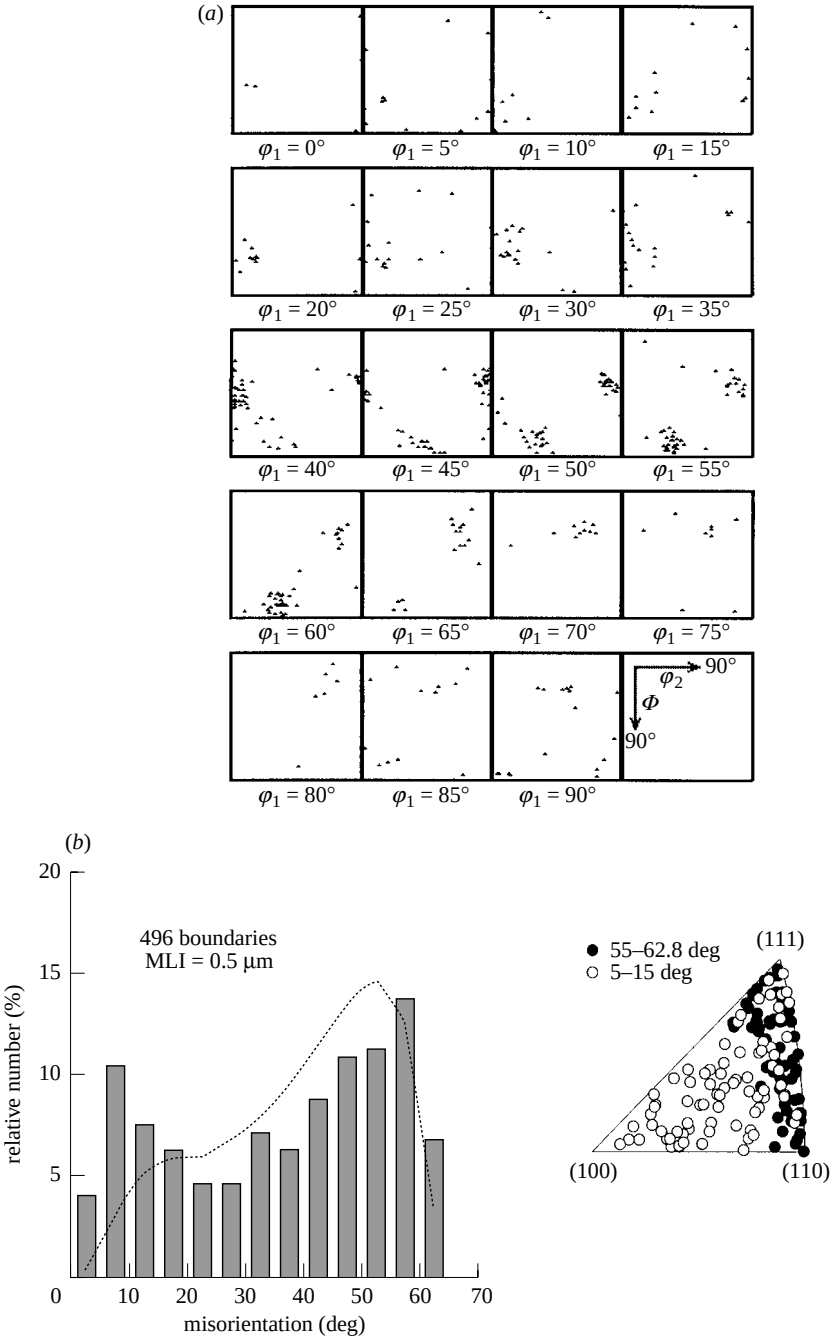

Figure 4. Microtexture data for as-processed Supral 2004. (*a*) Discrete Euler plot showing main texture components. (*b*) Misorientation data; in the histogram, the correlated misorientation distribution is shown by the bars while the uncorrelated distribution is represented by the dotted curve; the distribution of the rotation axes for the MMBs and HABs is shown as the GMT.

Downloaded from rsta.royalsocietypublishing.org

lar dislocation structure. Comparison of the correlated misorientation data with the corresponding uncorrelated misorientation data (the latter indicated by the dotted curve plotted with the histogram) indicates that the populations of boundaries misoriented by 0–15° and by 55–62.8° exceed those predicted by texture considerations alone, while the population of boundaries of misorientation between 20 and 55° is less than the texture prediction. The grain misorientation texture (GMT) data for this processing condition are included in the inset at the right in figure 4*b* and show that the rotation axes for the moderately misoriented boundaries (MMBs) (boundaries of 5–15° misorientation, indicated by open symbols) are uniformly distributed within the unit triangle. The rotation axes for high-angle boundaries (HABs) of 55–62.8° misorientation, shown by the filled symbols in the inset, are uniformly distributed along the arc of the symmetry boundary from (111) to (110). It should be noted that the rotation axes for such HABs cannot be located near (100) as a consequence of the definition of the misorientation angle as the minimum when symmetry is taken into account (Mackenzie 1964).

Microtexture data for material given annealing treatments for times varying from 30 min to 12 h at 450 °C are provided in figures 5 and 6. The discrete Euler plots in figure 5 show that the deformation texture of the as-processed condition is retained during annealing at 450 °C for times up to 12 h. The texture becomes slightly sharper and the relative populations of the various orientations have shifted somewhat, but no new texture components have become apparent. The bimodal nature of the grain-boundary misorientation distribution is also retained throughout these annealing treatments, as shown by the bars in the histograms of figure 6. Throughout these annealing treatments the populations of boundaries misoriented by 0–15° and by 55–62.8° exceed the predictions based on texture, and, furthermore, appear to increase with annealing time, while the relative numbers of boundaries misoriented by 20–50° undergo decreases. For the longest annealing time (12 h) the uncorrelated misorientation distribution also shows two distinct peaks (at 10–15° and 55–60°), which probably reflects the sharpening of texture and the reduced spread about the orientations of the main texture components. For this annealing time the correlated and uncorrelated misorientation distributions appear to coincide closely, except for boundaries misoriented by less than 10°. The rotation axes for the MMBs remain randomly distributed in the unit triangle of the GMT throughout these annealing treatments while the rotation axes for the HABs misoriented by 55–62.8° always tend to be uniformly distributed along the (111)–(110) symmetry boundary.

The ratios of the correlated to uncorrelated distributions are plotted versus misorientation angle in figure 7, which includes data for the as-processed and all of the processed and annealed conditions of this material examined here. This representation of the misorientation data emphasizes the extent to which the populations of boundaries in the misorientation ranges 0–15° and 55–62.8° exceeds those expected based on texture alone. The ratio of the number of boundaries by misorientation correlated to account for the texture present to the number uncorrelated to texture (the random distribution) is not strongly affected by annealing for times up to 6 h. For longer annealing periods of up to 12 h the aforementioned ratio tends to 1.0.

Typical times encountered in heating and superplastic straining and forming of components range from 30 min to perhaps 2 h. Thus it may be surmised for the Supral alloy investigated that the boundary misorientation distribution at the initiation of superplastic straining is essentially that developed by the prior deformation process-

PHILOSOPHICAL TRANSACTIONS OF THE ROYAL SOCIETY A MATHEMATICAL, PHYSICAL & ENGINEERING SCIENCES

PHILOSOPHICAL TRANSACTIONS OF THE ROYAL SOCIETY A MATHEMATICAL, PHYSICAL & ENGINEERING SCIENCES

Downloaded from rsta.royalsocietypublishing.org

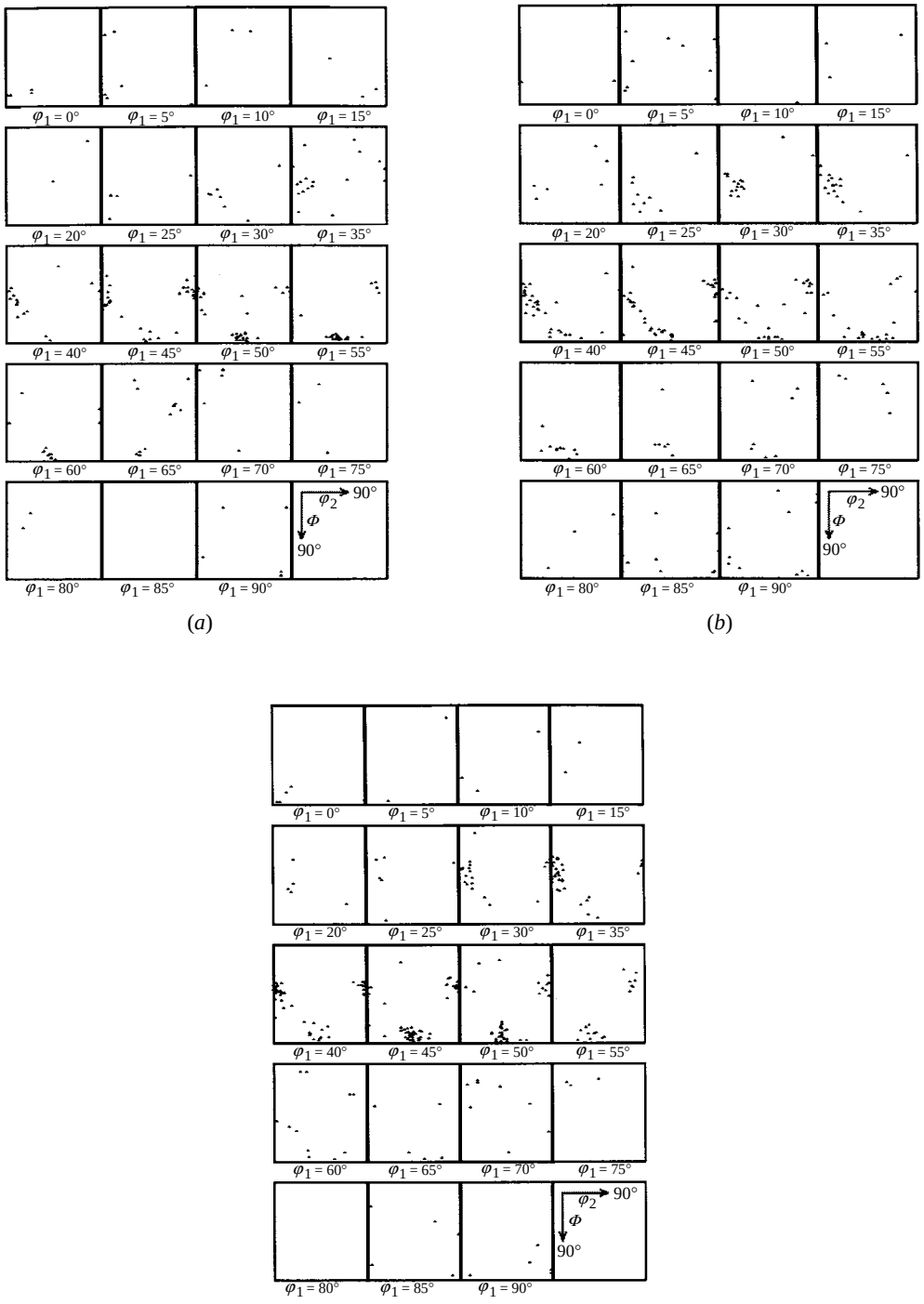

Figure 5. Discrete Euler plots for annealed Supral 2004, showing the main texture components after (*a*) 30 min, (*b*) 6 h and (*c*) 12 h at 450 °C.

PHILOSOPHICAL TRANSACTIONS OF THE ROYAL SOCIETY A MATHEMATICAL, PHYSICAL & ENGINEERING SCIENCES
PHILOSOPHICAL TRANSACTIONS OF THE ROYAL SOCIETY A MATHEMATICAL, PHYSICAL & ENGINEERING SCIENCES

Downloaded from rsta.royalsocietypublishing.org

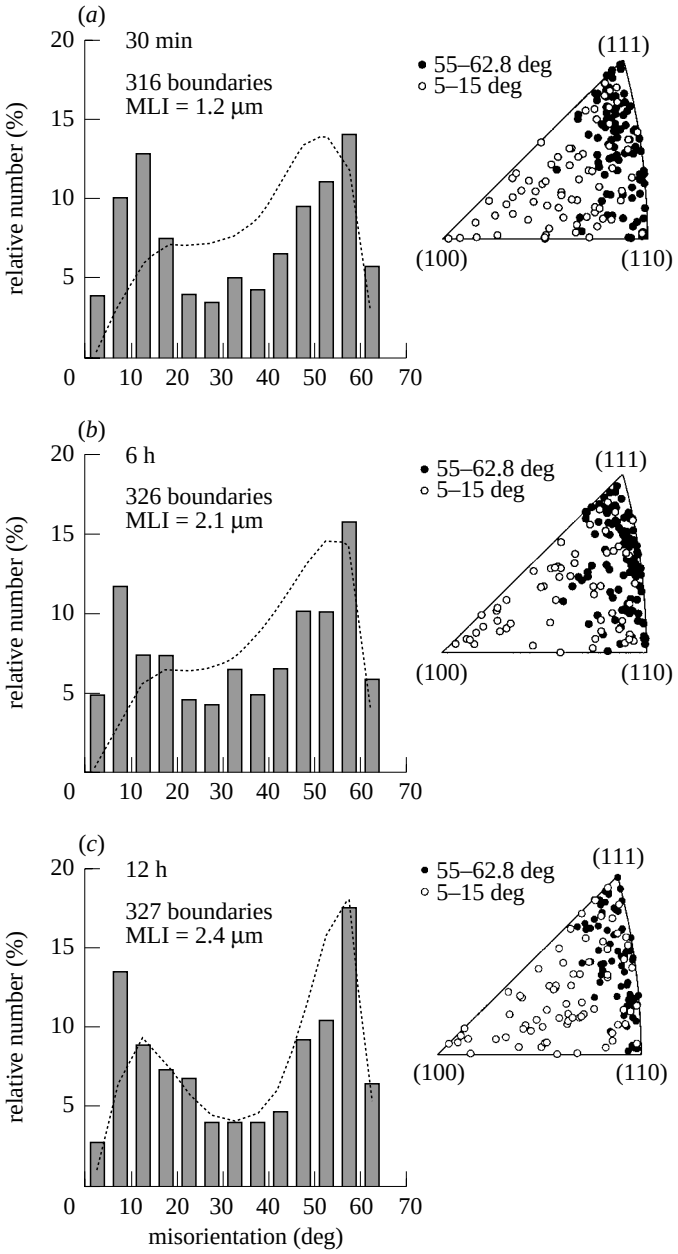

Figure 6. Misorientation data for annealing of Supral 2004 at 450 °C: (*a*) annealed for 30 min, (*b*) annealed for 6 h, and (*c*) annealed for 12 h. The correlated misorientation distribution is shown by the bars while the corresponding uncorrelated distribution is shown by the dotted curves. The GMTs show the distribution of the rotation axes for MMBs and HABs.

ing of the material, i.e. it is that of the deformation-induced cellular microstructure in the as-processed condition. This suggests that recovery during continuous recrystallization essentially involves the sharpening and retention of some cell walls

Downloaded from rsta.royalsocietypublishing.org

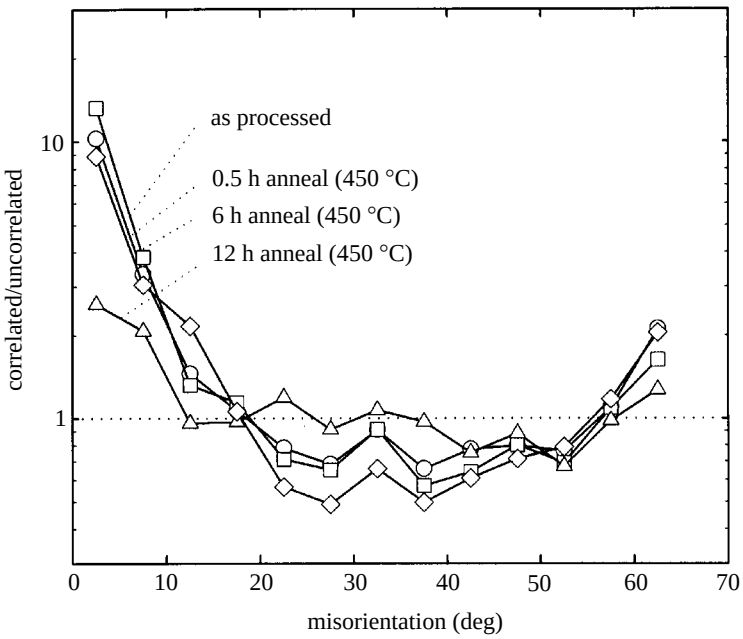

Figure 7. The effect of annealing for various times at 450 °C on the misorientation distribution, in terms of the ratio of the correlated to the uncorrelated populations, for Supral 2004.

from the deformation microstructure developed during prior deformation processing. The appearance and coarsening of a distinct (sub)grain structure during annealing indicates that many of the boundaries developed during processing are lost due to coalescence and annihilation as this growth occurs, but in a manner consistent with the texture present in the material.

5. Discussion

In this section, the HABs observed in the misorientation distribution of the as-processed alloy will be interpreted as interfaces between symmetric variants of certain deformation texture components. These components reflect deformation banding during prior processing. Then the low-angle boundaries (LABs, 0–5° misorientation) and MMBs are those of a cellular, deformation-induced structure located within these bands. Deformation banding has been described as a process of grain subdivision wherein the lattice rotates in different senses in adjacent regions (Lee *et al*. 1993; Lee & Duggan 1993; Kulkarni *et al*. 1998). Its potential importance as a deformation mechanism has long been recognized (Barrett 1939; Barrett & Levenson 1940). Its occurrence during rolling deformation may allow the grain as a whole to deform in plane strain although plane-strain conditions may not be met in each band. Less work is done by slip within each band than would be done by homogeneous slip but this requires that the bands be arranged so that the net strain in a group of bands meets the overall strain. Each band may have as few as two active slip systems such that deformation may occur in the absence of lattice rotation (Lee *et al*. 1993; Lee & Duggan 1993). In the present work, deformation banding can account for the distribution of HABs in this superplastic aluminium alloy, including the distribution of

Downloaded from rsta.royalsocietypublishing.org

Table 2. *Euler angles for the symmetric variants of the Br and nearby texture components*

component	designation (rolling plane)[rolling direction]	ϕ_1 (deg)	Φ (deg)	ϕ_2 (deg)
Br_1	$(110)\,[1\bar{1}2]$	55	90	45
Br_2	$(011)\,[2\bar{1}1]$	35	45	0
$Br(R_1)_1$	$(110)\,[3\bar{3}5]$	50	90	45
$Br(R_1)_2$	$(011)\,[5\bar{3}3]$	40	45	0
$Br(R_2)_1$	$(110)\,[3\bar{2}3]$	45	90	45
$Br(R_2)_2$	$(011)\,[3\bar{2}2]$	45	45	0

rotation axes for these boundaries, if it is assumed that adjacent bands correspond to variants of the deformation texture present in the material. This approach has also been successfully employed to describe the misorientation distribution in an Al–Ca–Zn alloy that also transforms by a continuous recrystallization reaction (Pérez-Prado *et al*. 1998).

(*a*) *The high-angle boundaries*

Based on observations in severely deformed pure metals, it has been proposed that geometrically necessary grain boundaries may reflect misorientations related to the texture while incidental dislocation boundaries reflect random dislocation interactions (Hughes & Hansen 1997). In an investigation of continuous recrystallization of an Al–Fe–V alloy it was concluded that the population of HABs is higher than expected from texture considerations and, furthermore, that many of these were interfaces between twin-related variants of the texture (Davies *et al*. 1997). A similar conclusion was reported in work on a rolled Al–Cu–Li alloy (Hales & Crooks 1997). It is implicit in the deformation banding model (Lee *et al*. 1993; Lee & Duggan 1993) that the lattice within a band, many of which may form within an individual grain, rotates toward a stable end orientation during severe deformation and that the lattice within an adjacent band rotates toward a symmetric orientation. In the present work, this would suggest that the misorientation distribution of the HABs may be related to the orientation distribution of the texture. Here, examination of the discrete Euler data for the as-processed and all of the processed and annealed conditions shows that there are orientations located at both variants of the Br component and nearby orientations which are distributed along lines of Φ = const., especially the α-fibres. These latter orientations are at positions that are rotated about the sheet normal (i.e. about $\langle 110 \rangle$) relative to Br. Figure 8 is a schematic representation of the fundamental zone of Euler space for a cubic material showing the two variants of Br (denoted Br_1 and Br_2) and nearby regions containing most of the experimentally observed orientations. These regions are symmetrically related to each other by the orthotropic symmetry of the rolled sheet. The Euler angles for the two Br variants and two more nearby components lying along the α-fibres, here designated $Br(R_1)$ and $Br(R_2)$, are provided in table 2.

These latter components are related by successive 5° rotations from Br about the sheet normal, corresponding to the 5° increments in the discrete Euler plots of figures 4 and 5.

Downloaded from rsta.royalsocietypublishing.org

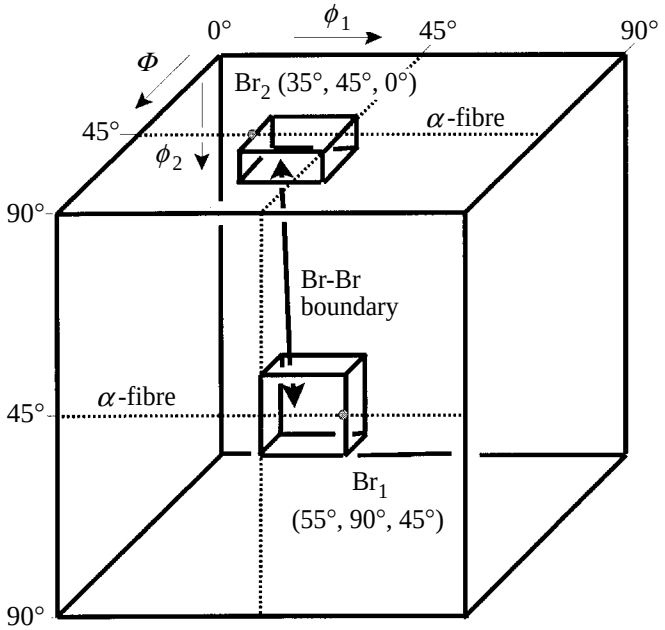

Figure 8. The fundamental zone of Euler space showing the regions near the two distinct Br variants in which most orientations are distributed in the texture of Supral 2004. A correlated misorientation distribution may be calculated by assuming that adjacent grains lie alternately in locations distributed throughout the Br_1 or Br_2 regions; the misorientation of the resulting interface is represented by the arrow.

Figure 9 illustrates concisely the effect of including this spread of orientations along α-fibres into a model of grain boundaries as interfaces between such texture variants; the ideal orientations for the two distinct variants of each of the three Br-related components of table 2 are depicted in {111} pole figures. For the Br component, the two distinct variants, Br_1 and Br_2, are related to each other by a 60° rotation about a ⟨111⟩ axis; indeed, the particular rotation axis is that which lies parallel to the transverse direction (TD) of the rolled sheet. This 60°/⟨111⟩ rotation about the TD is equivalent to the effect of a mirror plane normal to the TD (one of the elements of the orthotropic symmetry of the rolled sheet). This may also be described as a Σ3 coincidence site lattice (CSL) boundary. The symmetric variants of $Br(R_1)$, namely $Br(R_1)_1$ and $Br(R_1)_2$, are related by a 60.6° rotation about a ⟨332⟩ axis. Furthermore, the symmetric variants of the third component in table 2, $Br(R_2)_1$ and $Br(R_2)_2$, are related by a rotation of 62.7° about a ⟨552⟩ direction. Additional possible misorientations are indicated in figure 8, such as that between Br_1 and $Br(R_2)_2$, 60.6° about a ⟨221⟩, and small rotations of either 5 or 10° about a ⟨110⟩ (specifically, the sheet normal, N). It is noteworthy that all of the rotation axes for all of these HABs in figure 9 are distributed along the (111)–(110) symmetry boundary. It should also be noted that there are few MMBs (misorientations of 5–15°) observed with rotation axes near (110) in the GMTs of figures 4 and 6.

The rotation axes predicted in figure 9 for boundaries between these symmetric orientations would lie exactly on the (111)–(110) symmetry boundary. In figures 4 and 6 the majority of the rotation axes are distributed within the inverse stereographic

Downloaded from rsta.royalsocietypublishing.org

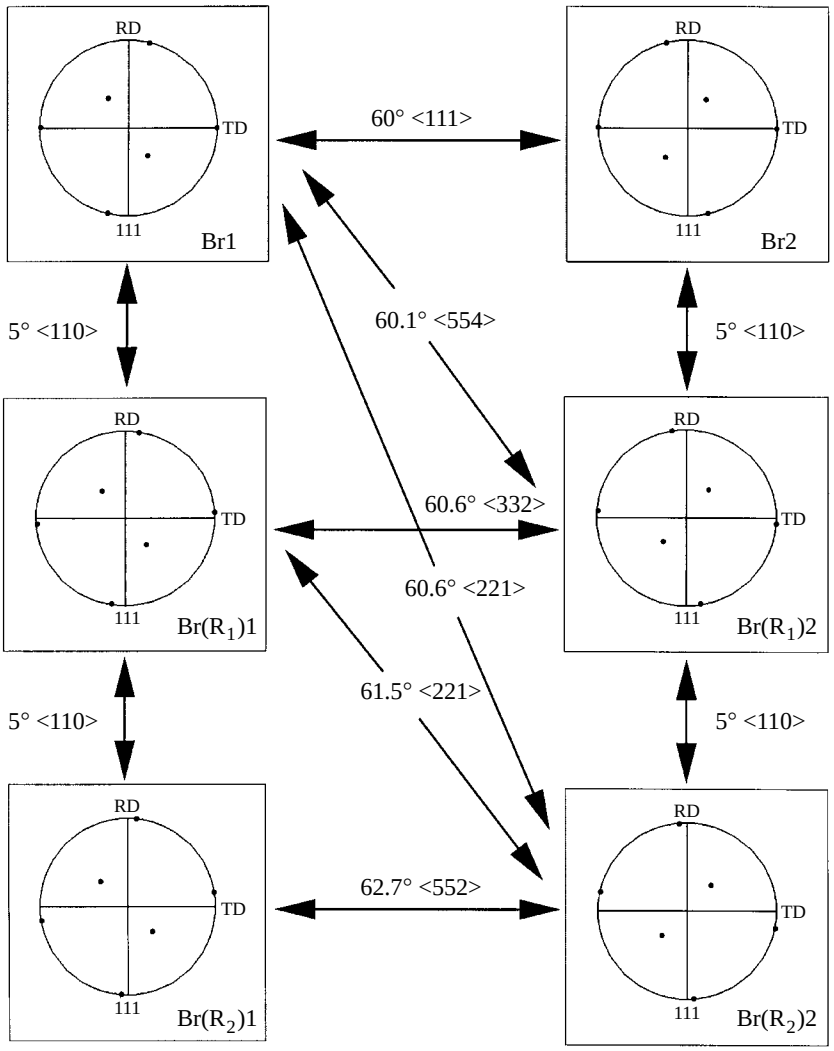

Figure 9. A schematic illustrating the relative locations on {111} pole figures of the symmetric variants for the main texture components present in Supral 2004, and the corresponding axis/angle pairs of the boundaries separating grains oriented as symmetric variants.

triangle of the GMT. This suggests that most of the actual crystallite orientations are rotated slightly away from the α-fibre. In the absence of a detailed model for the distribution of these orientations it was assumed that these crystallite orientations were uniformly distributed throughout the regions near the exact Br_1 and Br_2 orientations indicated in figure 8. Then, it was assumed that adjacent grain orientations lay alternately within these regions and that the grain-to-grain misorientations could be calculated as suggested by the arrow in figure 8. Grain orientations were assumed to be represented by a grid of equally spaced points in each of these regions and a distribution was determined by calculating the angles and axes of misorientation for an orientation in one variant with respect to all orientations in the symmetric

Downloaded from rsta.royalsocietypublishing.org

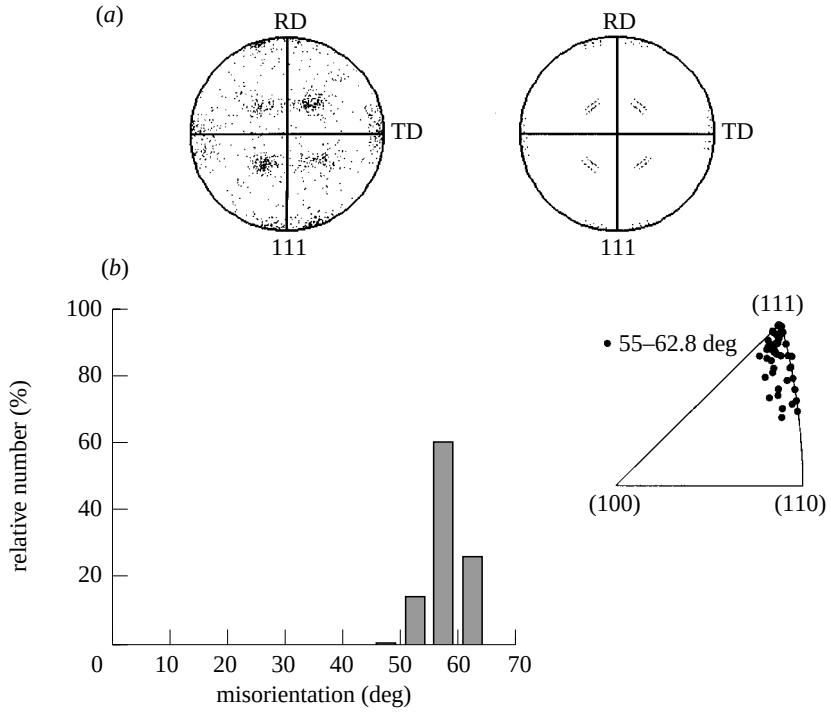

Figure 10. The discrete pole figures in (*a*) show the measured {111} texture of Supral 2004 (annealed for 30 min at 450 °C) in comparison with the distribution of {111} poles for orientations distributed in the Br_1 and Br_2 regions in figure 8. In (*b*), the calculated misorientation distribution and GMT for grains oriented as symmetric variants of Br_1 and Br_2 are shown.

variant. The elements of the orientation matrices for this calculation were as follows:

$$\left.\begin{aligned}
a_{11} &= \cos\phi_1 \cos\phi_2 + \sin\phi_1 \cos\Phi \sin\phi_2,\\
a_{12} &= \cos\phi_1 \sin\phi_2 - \sin\phi_1 \cos\Phi \cos\phi_2,\\
a_{13} &= -\sin\phi_1 \sin\Phi,\\
a_{21} &= \sin\phi_1 \cos\phi_2 - \cos\phi_1 \cos\Phi \sin\phi_2,\\
a_{22} &= \sin\phi_1 \sin\phi_2 + \cos\phi_1 \cos\Phi \cos\phi_2,\\
a_{23} &= \cos\phi_1 \sin\Phi,\\
a_{31} &= \sin\Phi \sin\phi_2,\\
a_{32} &= -\sin\Phi \cos\phi_2,\\
a_{33} &= \cos\Phi.
\end{aligned}\right\} \qquad (5.1)$$

The misorientation matrices and the misorientation angles and corresponding rotation axes were then calculated according to equations (3.2) and (3.3).

Figure 10 summarizes the results of these calculations for the regions depicted in figure 8, which extend 5° into the fundamental zone. In figure 10*a* the experimentally determined discrete {111} pole figure for Supral, annealed for 30 min at 450 °C, is compared with the distribution of the {111} poles for orientations distributed in the Br_1 and Br_2 regions of figure 8 and the calculated misorientation distribution and GMT is shown in figure 10*b*. For the assumed distribution of orientations the spread

Downloaded from rsta.royalsocietypublishing.org

is somewhat less than that seen in the experimental pole figure. The corresponding misorientation distribution is more sharply peaked at 55–60° than those of figures 4 and 6 although this analysis does predict a spread in misorientations from 45° up to 62.8°. The spread of rotation axes along the (111)–(110) symmetry boundary is less than observed experimentally, while the spread into the unit triangle corresponds more closely to the experimental results.

(*b*) *The low-angle and moderately misoriented boundaries*

The bimodal misorientation distributions have been modelled following an approach involving grain subdivision by dislocation reaction (Hughes & Hansen 1997). The model includes contributions for the boundaries of the deformation-induced cellular dislocation structure produced by rolling as well as for the HABs that are interfaces between the symmetric variants of the Br-related texture components here. For boundaries that develop as a result of random dislocation interaction, an empirical probability density distribution of the form,

$$h(u) = au^n \exp(-u^{n-1}), \tag{5.2}$$

was suggested, where u $(= \theta/\theta_{\mathrm{ave}})$ is the ratio between the misorientation, θ, and an average misorientation, θ_{ave}, n is an exponent and a is a constant. This was shown (Hughes & Hansen 1997) to represent the probability distribution of the deformation-induced dislocation boundaries in several severely deformed pure metals. Such a distribution evidently reflects a build-up in the misorientations of cell walls due to dislocation interactions that occur during the straining of rolling and, in many cases, observed distributions of misorientation angles were well-described by $n = 2$ and values of θ_{ave} in the range 10–15°. Such a function indicates that the misorientation distributions are self-similar when θ_{ave} contains all of the strain dependence (Hughes & Hansen 1997).

Here several similar distribution functions have been used to fit the experimental data corresponding to both the as-processed and the processed and annealed material. The goodness of fits was evaluated by means of the correlation coefficient, i.e. the R-value, and it was found that the Rayleigh distribution,

$$h(u) = au^{n-1} \exp(-u^n), \tag{5.3}$$

was somewhat better suited to fit the experimental data, since it gave the highest R-value for all cases examined here. The values of the average misorientation, θ_{ave}, are included in the upper plot of figure 10. Best fits (highest R-values) were obtained for $n = 2$. These average misorientation values are very similar to and in both cases slightly larger than those reported in work on pure aluminium (Hughes & Hansen 1997). This is not surprising in view of the alloy additions in Supral 2004 and other continuously recrystallizing alloys (McNelley & McMahon 1996*a*, *b*; McNelley & McMahon 1997; Pérez-Prado *et al*. 1998). Since the values of the fitting parameters are very similar in all cases, it is possible to model all distributions of moderately misoriented boundaries by means of the same Rayleigh distribution. The result is shown in figure 11*b*. The portion of the histogram corresponding to misorientations up to 30° was obtained by integration of a Rayleigh distribution using values of $\theta_{\mathrm{ave}} = 15.8°$ and $n = 2$. From experimental data, boundaries of misorientation $\theta <$ 30° comprise *ca.* 40% of all boundaries (depending on the extent of annealing) while the remaining 60% are misoriented by $\theta \geqslant 30°$. Accordingly a histogram representing

Downloaded from rsta.royalsocietypublishing.org

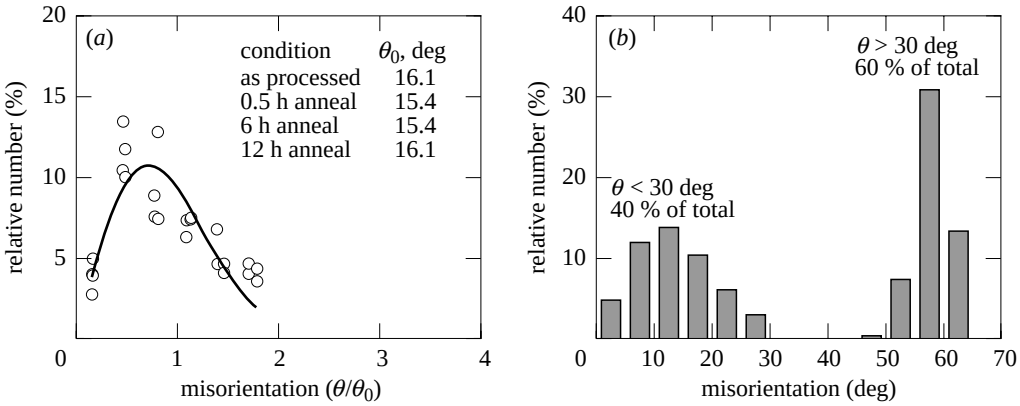

Figure 11. The misorientation distribution may be modelled in two parts. In (*a*), the distribution for $\theta < 30^\circ$ is fitted by a probability density distribution of the form $h(\theta) = au\exp(-u^2)$, where a is a constant and $u = \theta/\theta_0$; this is combined in (*b*) with the misorientation distribution for HABs as symmetric variants of the texture. It is assumed that boundaries of $\theta > 30^\circ$ constitute 60% of the total while those with $\theta < 30^\circ$ constitute 40% of the total.

the complete distribution was plotted by scaling the data for $\theta < 30^\circ$ and $\theta \geqslant 30^\circ$ (figure 10*b*). The result is shown in figure 11*b*.

Finally, a schematic model of the deformation microstructure of this alloy, including the effect of annealing, is shown in figure 12. Following analysis of deformation banding (Lee *et al*. 1993; Lee & Duggan 1993) it is assumed that multiple bands form within each grain; this is consistent with a spacing (MLI) value of 0.5 µm in as-processed material although the original grains were reduced to a thickness of *ca*. 3.0 µm. Adjacent bands would have lattice orientations corresponding to the symmetric variants of the Br and nearby orientations, as suggested in figure 12; a cellular structure is indicated such that the number of cell and variant boundaries crossed during a linear traverse is similar. It is also suggested that lattice curvature is reduced during annealing and that some cell boundaries are annihilated during annealing, but in a manner that preserves the distribution of orientations about the main texture components as reflected in the orientations of the variants themselves. Finally, it has been noted (Lee *et al*. 1993; Lee & Duggan 1993) that such a banded structure may deform with only two active slip systems in each band while each band remains compatible with its neighbours. This allows large deformations to occur while retaining a stable lattice orientation.

6. Conclusions

The microstructure, microtexture and misorientation distributions of the as-processed commercial Supral 2004 alloy have been examined by EBSP methods in the as-processed condition and after annealing at 450 °C for periods ranging from 30 min to 12 h. The following conclusions and implications may be drawn from this study.

1. The microtexture of Supral 2004 both in the as-processed and in the processed and annealed conditions consists primarily of deformation texture components. There is no evidence of recrystallization components associated with the formation of new grains by HAB migration during post-TMP annealing.

Downloaded from rsta.royalsocietypublishing.org

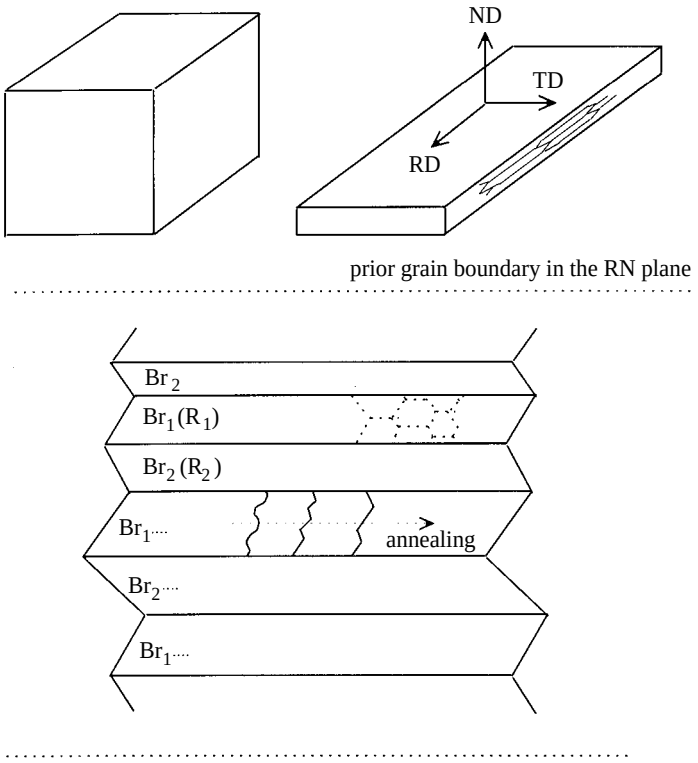

Figure 12. A schematic of banding in the RN plane during the plane-strain deformation of rolling (upper diagram). The bands (lower diagram) reflect lattice rotation toward stable end orientations near the symmetric Br orientations; HABs in the misorientation distribution are interfaces between the bands. LABs and MMBs form by dislocation reactions within bands. During annealing, recovery is reflected in reduction of lattice curvature by formation of boundaries; coarsening of the structure by annihilation of the boundaries occurs in a manner consistent with the preservation of the end orientations of the texture.

2. The continuous recrystallization reaction in Supral 2004 results in grain-boundary misorientation distributions which are bimodal in nature with a predominance of HABs (55–62.8°) and MMBs (10–15°). The HABs can be modelled as interfaces between symmetric variants of the main texture components. These boundaries were developed in the as-processed material in association with deformation banding and are retained during annealing. The MMBs are deformation-induced dislocation boundaries and result from dislocation interaction during large-strain deformation processing. The distribution of these boundaries may be modelled by means of a Rayleigh distribution.

3. In engineering aluminium alloys, microstructures associated with continuous recrystallization reactions enable superplastic response at lower temperatures and higher strain rates than those formed as a result of discontinuous recrystallization reactions. Better models of microstructural development during deformation processing are required in order to enable superplastic response in a wider range of aluminium alloys. These models must consider dislocation

Downloaded from rsta.royalsocietypublishing.org

reactions leading to substructure development and cell formation, deformation banding and the roles of both fine and coarse particles. The factors that influence the stability of deformation-induced structures, which dictate either inhomogeneous or homogeneous recrystallization reactions during subsequent annealing and elevated temperature straining, also require clarification.

M.T.P. acknowledges the Spanish Ministry of Education for an FPI travel grant.

References

Adams, B. L. 1986 Description of the intercrystalline structure distribution in polycrystalline metals. *Metall. Trans.* A **17**, 2199–2207.

Barrett, C. S. 1939 The structure of iron after compression. *Trans. Am. Inst. Min. Engrs* **135**, 296–309.

Barrett, C. S. & Levenson, L. H. 1940 The structure of aluminum after compression. *Trans. Am. Inst. Min. Engrs* **137**, 112–127.

Bricknell, R. H. & Edington, J. W. 1979 Textures in a superplastic Al–6Cu–0.3Zr alloy. *Acta Metall.* **27**, 1303–1311.

Bunge, H. J. 1982 *Texture analysis in materials science.* London: Butterworths.

Davies, R. K., Randle, V. & Marshall, G. J. 1997 The evolution of microstructure and texture in a continuously recrystallised commercial Al–Fe–Si alloy. In *ReX96, Proc. 3rd Int. Conf. on Recrystallization and Related Phenomena, MIAS, Monterey, CA* (ed. T. R. McNelley), pp. 271–278.

Doherty, R. D., Gottsttein, G., Hirsch, J., Hutchinson, W. B., Lucke, K., Nes, E. & Wilbrandt, P. J. 1988 Report of panel on recrystallization textures: mechanisms and experiments. In *Proc. ICTOM 8* (ed. J. S. Kallend & G. Gottstein), pp. 563–572. Warrendale, PA: TMS.

Doherty, R. D., Hughes, D. A., Humphreys, F. J., Jonas, J. J., Juul Jensen, D., Kassner, M. E., King, W. E., McNelley, T. R., McQueen, H. J. & Rollett, A. D. 1997 Current issues in recrystallization: a review. *Mater. Sci. Engng* A **238**, 219–274.

Edington, J. W. 1982 Microstructural aspects of superplasticity. *Metall. Trans.* A **13**, 703–715.

Grimes, R. 1988 The manufacture of superplastic alloys. In *Superplasticity. NATO-Advisory Group for Aerospace Research and Development (AGARD).* Lecture Series no. 168, pp. 8.1–8.16.

Hales, S. J. & Crooks, R. 1997 Recrystallized and unrecrystallized Al–Li alloys for elevated temperature service. In *ReX96, Proc. 3rd Int. Conf. on Recrystallization and Related Phenomena, MIAS, Monterey, CA* (ed. T. R. McNelley), pp. 511–518.

Hughes, D. A. & Hansen, N. 1997 High angle grain boundaries formed by grain subdivision mechanisms. *Acta Mater.* **45**, 3871–3886.

Humphreys, F. J. 1977 The nucleation of recrystallization at second phase particles in deformed aluminum. *Acta Metall.* **25**, 1323–1344.

Humphreys, F. J. 1997 A unified theory of recovery, recrystallization and grain growth, based on the stability of cellular microstructures. I. The basic model. *Acta Mater.* **45**, 4231–4240.

Kulkarni, S. S., Starke, E. A. & Kujlmann-Wilsdorf, D. 1998 Some observations on deformation banding and correlated microstructures of two aluminum alloys compressed at different temperatures and strain rates. *Acta Mater.* **46**, 5283–5301.

Lee, C. S. & Duggan, B. J. 1993 Deformation banding and copper-type rolling textures. *Acta Mater.* **41**, 2691–2699.

Lee, C. S., Duggan, B. J. & Smallman, R. E. 1993 A theory of deformation banding in cold rolling. *Acta Mater.* **41**, 2265–2270.

Downloaded from rsta.royalsocietypublishing.org

Mackenzie, J. K. 1964 The distribution of rotation axes in a random aggregate of cubic crystals. *Acta Metall.* **12**, 223–235.

McMahon, M. E. 1996 Grain boundary development in superplastic aluminum alloys. PhD dissertation, Naval Postgraduate School, Monterey, CA, USA.

McNelley, T. R. & McMahon, M. E. 1996*a* Analyzing superplastic microstructures using interactive EBSP methods. *J. Met.* **48**, 58–60.

McNelley, T. R. & McMahon, M. E. 1996*b* An investigation by interactive electron backscatter pattern analysis of processing and superplasticity in an aluminum–magnesium alloy. *Metall. Mater. Trans.* A **27**, 2252–2262.

McNelley, T. R. & McMahon, M. E. 1997 Microtexture and grain boundary evolution during microstructural refinement processes in SUPRAL 2004. *Metall. Mater. Trans.* A **28**, 1879–1887.

McNelley, T. R., McMahon, M. E. & Hales, S. J. 1997 An EBSP investigation of alternate microstructures for superplasticity in aluminum–magnesium alloys. *Scri. Mater.* **36**, 369–375.

Nieh, T. G., Wadsworth, J. & Sherby, O. D. 1997 *Superplasticity in metals and ceramics*. Cambridge University Press.

Paton, N. E. & Hamilton, C. H. 1978 Method of imparting a fine grain structure to aluminum alloys having precipitating constituents. US Patent 4 092 181.

Pérez-Prado, M. T., McNelley, T. R., Ruano, O. A. & González-Doncel, G. 1998 Microtexture evolution during annealing and superplastic deformation of Al–5%Ca–5%Zn. *Metall. Mater. Trans.* A **29**, 485–492.

Pospiech, J., Sztwiertnia, J. & Haessner, F. 1986 The misorientation distribution function. *Texture Microstruct.* **6**, 205–215.

Randle, V. 1992 *Microtexture determination and its applications*. London: The Institute of Metals.

Sherby, O. D. & Burke, P. M. 1968 Mechanical behavior of crystalline solids at elevated temperature. *Prog. Mater. Sci.* **13**, 325–390.

Sherby, O. D. & Wadsworth, J. 1982 Development of fine-grain superplastic materials. In *Deformation Processing and Microstructure* (ed. G. Krauss), pp. 355–389. Metals Park, OH: American Society for Metals.

Watts, B. M., Stowell, M. J., Baike, B. L. & Owen, D. G. E. 1976 Superplasticity in Al–Cu–Zr alloys. I. Material preparation and properties. *Metal Sci. J.* **10**, 189–197.

Wert, J. A., Paton, N. E., Hamilton, C. H. & Mahoney, M. W. 1981 Grain refinement in 7075 aluminum by thermomechanical processing. *Metall. Trans.* A **12**, 1267–1276.

Downloaded from rsta.royalsocietypublishing.org

PHILOSOPHICAL TRANSACTIONS OF THE ROYAL SOCIETY A MATHEMATICAL, PHYSICAL & ENGINEERING SCIENCES

PHILOSOPHICAL TRANSACTIONS OF THE ROYAL SOCIETY A MATHEMATICAL, PHYSICAL & ENGINEERING SCIENCES